- 16. SOFIA/HAWC+ Far-InfraRed Polarimetric Large Area CMZ Exploration (FIREPLACE) Survey I: General Results from the Pilot Program by Natalie O. Butterfiel et al. (ApJ)
- 17. SOFIA/HAWC+ Far-Infrared Polarimetric Large Area CMZ Exploration (FIREPLACE) II: Detection of a Magnetized Dust Ring in the Galactic Center, by Natalie O. Butterfield et al. (ApJ)
- 18. INvestigations of massive Filaments ANd sTar formation (INFANT). I. Core Identification and Core Mass Function by Yu Cheng, et al. (ApJ)
- 19. Mid-Infrared Spectrum of the Disk around the Forming Companion GQ Lup B Revealed by JWST/MIRI by Gabriele Cugno, et al.
- 20. JWST/NIRCam Imaging of Young Stellar Objects. II. Deep Constraints on Giant Planets and a Planet Candidate Outside of the Spiral Disk Around SAO 206462 by Gabriele Cugno, et al. (ApJ)
- 21. Climbing the Cliffs: Classifying YSOs in the Cosmic Cliffs JWST Data using a Probabilistic Random Forest by B. L. Crompvoets, et al. (ApJ)
- 22. Full orbital solutions in pre-main sequence high-order multiple systems: GG Tau Ab and UX Tau B, by Gaspard Duchêne, et al. (AAp)
- 23. Planet Formation by Gas-Assisted Accretion of Small Solids, by Gennaro D'Angelo, Peter Bodenheimer (ApJ)
- 24. The jet of BP Tau, by A. V. Dodin, et al. (AApL)
- 25. The stability of dense cores near the Serpens South protocluster, by Rachel K. Friesen, Emma Jarvis (ApJ)
- 26. MINDS: Mid-infrared atomic and molecular hydrogen lines in the inner disk around a low-mass star by Riccardo Franceschi, at al. (AAp)
- 27. An ALMA search for substructure and fragmentation in starless cores in Orion B North, by Samuel Fielder, et al. (ApJ)
- 28. A self-consistent model for dust settling and the vertical shear instability in protoplanetary disks, by Yuya Fukuhara, Satoshi Okuzumi (PASJ)
- 29. Gaia23bab : a new Exor, by T. Giannini, et al. (ApJ)
- 30. Reduction of dust radial drift by turbulence in protoplanetary disks, by Fabiola Antonietta Gerosa, et al. (AAp)

16. SOFIA/HAWC+ Far-InfraRed Polarimetric Large Area CMZ Exploration (FIREPLACE) Survey I: General Results from the Pilot Program by Natalie O. Butterfiel et al. (ApJ)

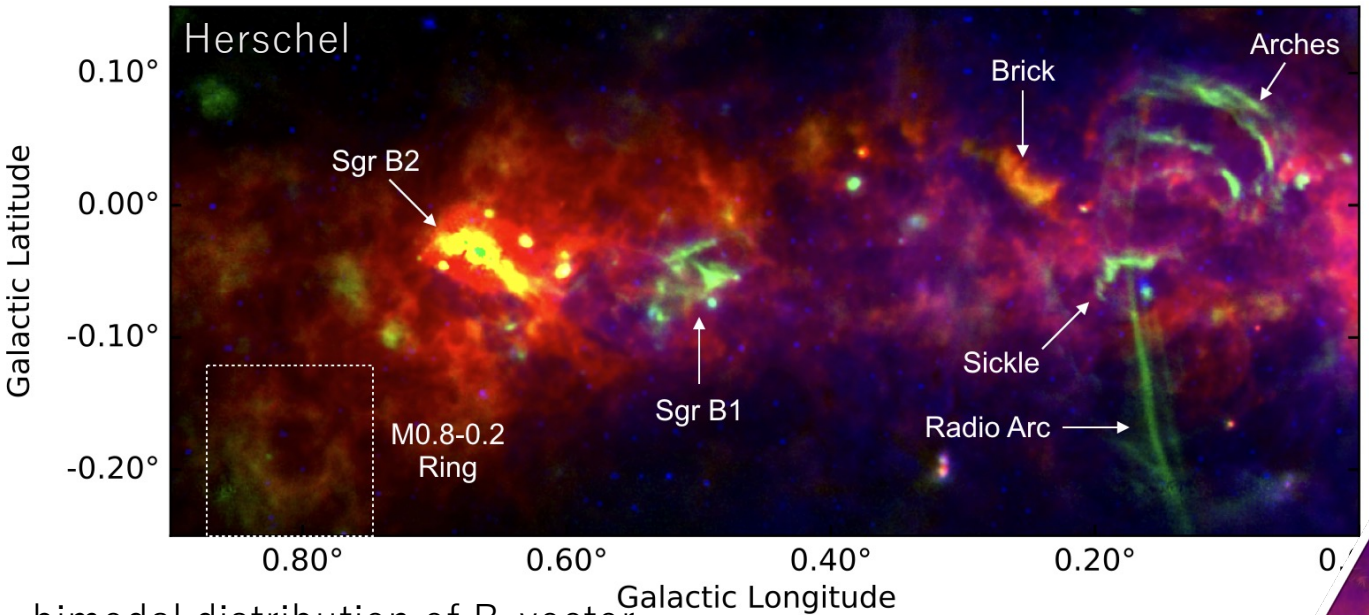

λ=214μm

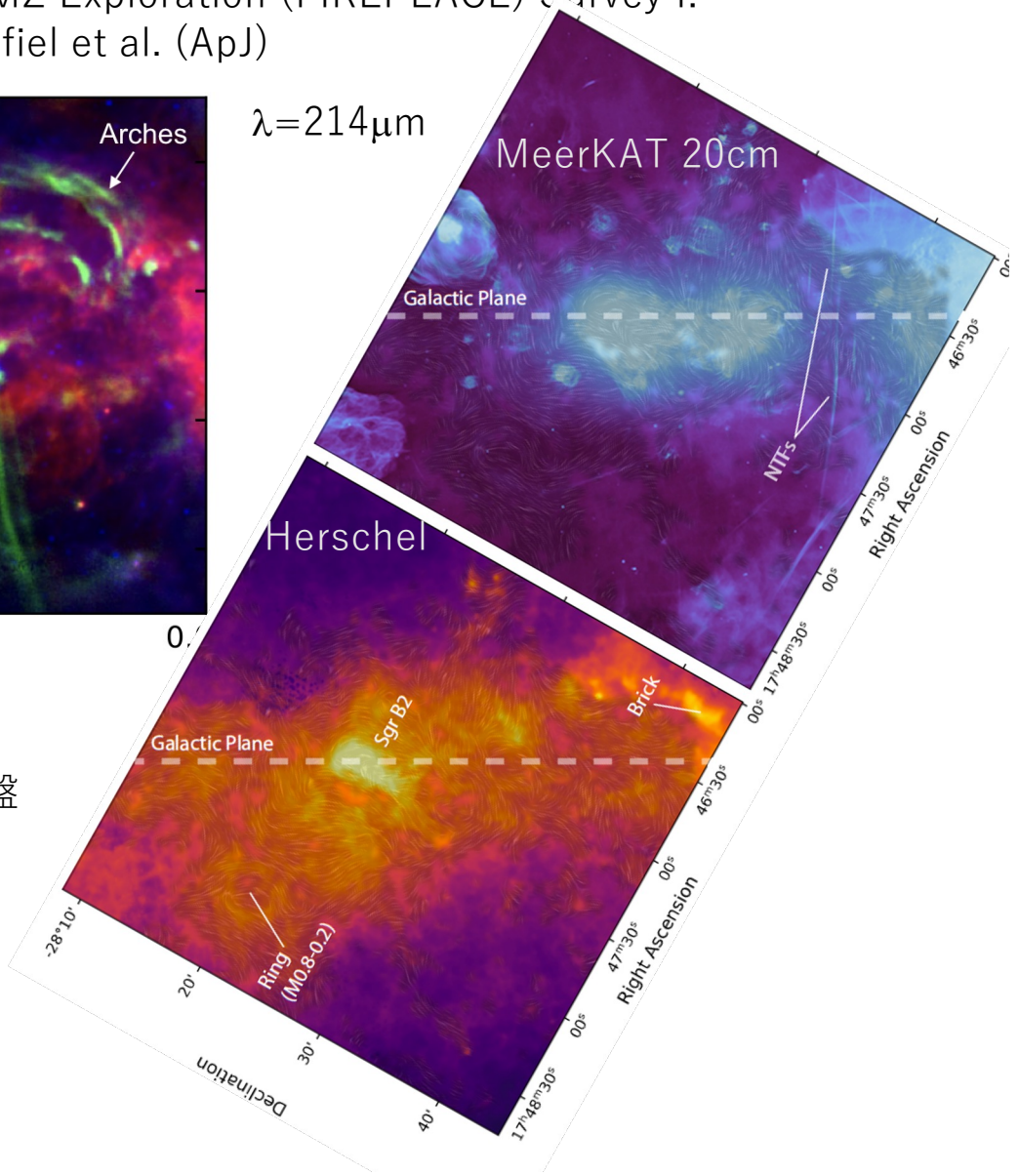

bimodal distribution of B-vector

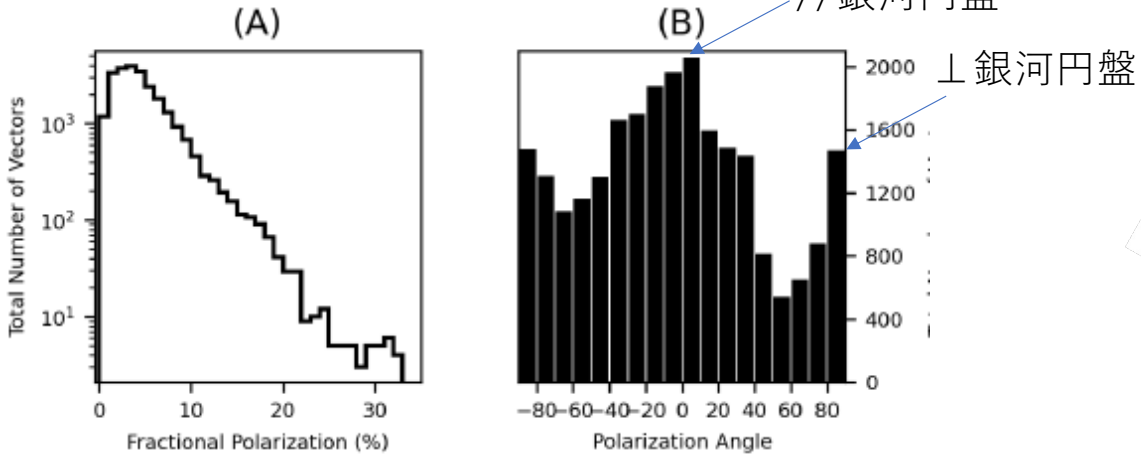

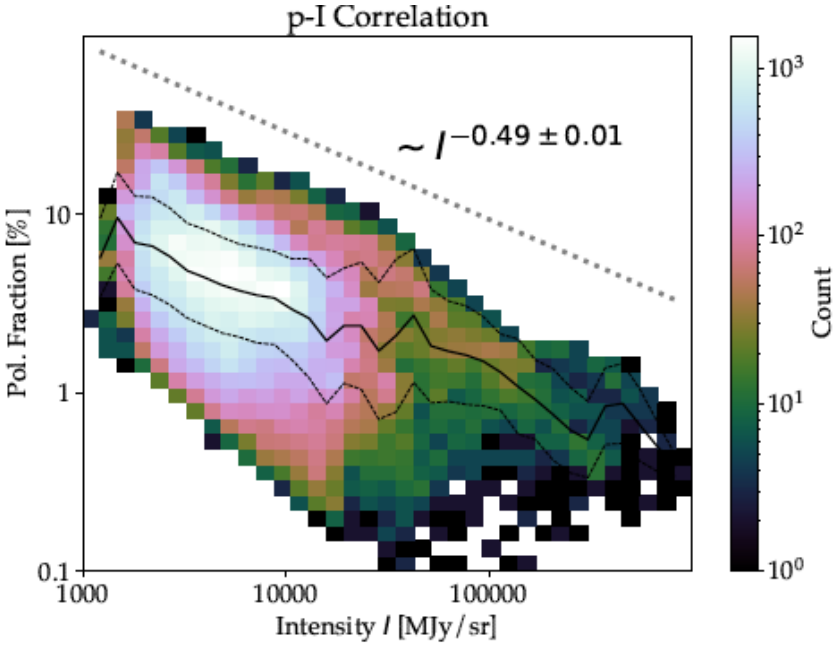

(1) loss of grain alignment in dense regions that are shielded from the interstellar radiation field (ISRF),
(2) magnetic field variation within the volume of the beam
(3) systematic effects due to sensitivity limitation and the nature of the Ricean distribution that describes the statistics of positive-definite quantities such as polarization (Pattle, K.+2019)

17. SOFIA/HAWC+ Far-Infrared Polarimetric Large Area CMZ Exploration (FIREPLACE) II: Detection of a Magnetized Dust Ring in the Galactic Center, by Natalie O. Butterfield et al. (ApJ)

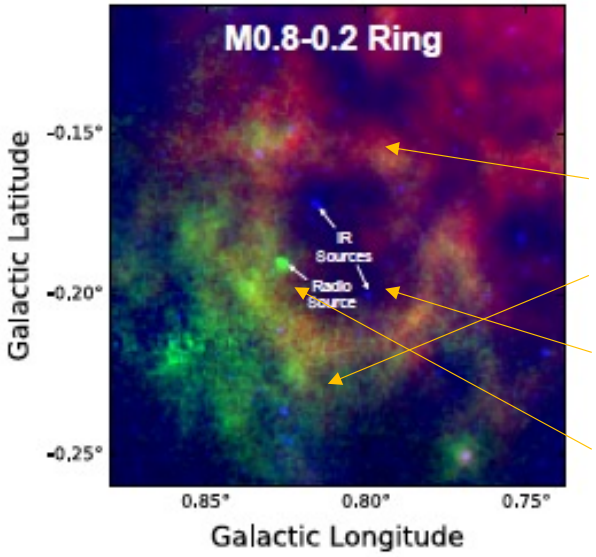

Green= 3mm (GBT) Red=160μm (Herschel) Blue= 8μm (Spitzer)

warmer dust

cold gas and thermal radio emission

two 8 μm point-sources,

a bright radio point-source,

a wind-blown feature or a supernova remnant fror SCUBA (Pierce-Price+2000)
--- from Nobeyama H13CO+/SiO,
T~4x10^49erg. 0.18Myr, 2700M$_\odot$(Tsuboi+2015

λ =214 μ mSofia/HAWCサーベイデータで B-RATモデルに則り、星間磁場を調べる

I強度弱いところまで引いた磁場ベクトル
（∝p%）
Iへ向かってpI/Iは↗
grain alignment↗？

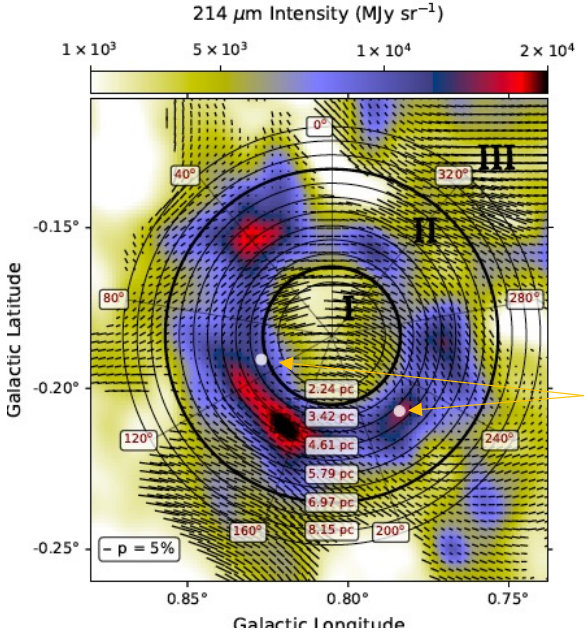

収束点

(l,b)➔(r,θ)

(l,b)➔(r,θ)

azimuth方向　　radial方向　　color: $I_{214\mu m}$

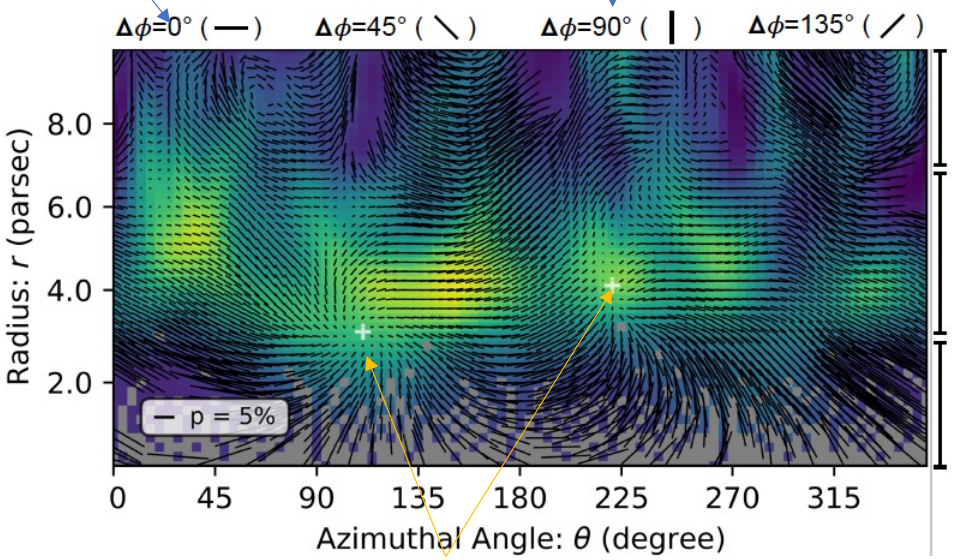

収束点

偏光度はIIが最大、IとIIIは低い。

Region III
exterior: less coherent
外側の磁場のパターン

Region II
ring: brightest + clumpy
5個程度のクランプ,Δϕ~0°　的

Region I
interior: well organized
into arc-like structure

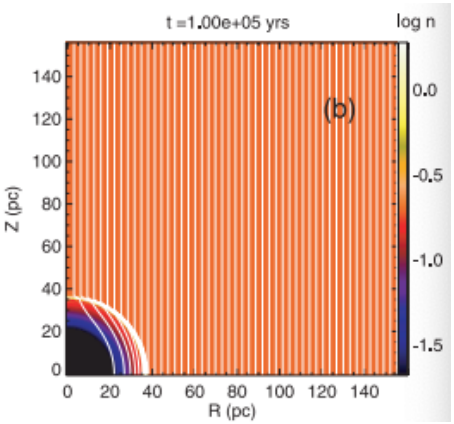

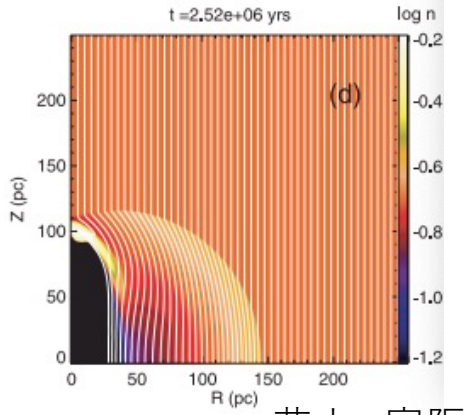

Nature
SNR/HII region
Synchrotron loss

$$\tau = 0.9 \times 10^5 \mathrm{yr} \left(\frac{B}{572\mu\mathrm{G}}\right)^{-3/2} \left(\frac{\nu_c}{1.28\mathrm{GHz}}\right)^{-1/2}$$

evolved SNR
↑ The lack of excess X-ray emission within and interior to the M0.8–0.2 ring (Chandra)

花山+富阪2006
B_0=5μG
n_0=0.2cm^{-3}
E_0=5x10^{50}erg

Davis-Chandrasekhar-Fermi (DCF) method

$$B_{\mathrm{POS}} = \sqrt{4\pi\rho_m}\sigma_v \left[\frac{\langle B_t^2\rangle}{\langle B_0^2\rangle}\right]^{-1/2}$$

$$\sigma_v = 1.91 \pm 0.01 \ \mathrm{km\ s^{-1}}$$

$$B_{\mathrm{POS}} = 572 \pm 12 \ \mu\mathrm{G}$$

18. INvestigations of massive Filaments ANd sTar formation (INFANT). I. Core Identification and Core Mass Function by Yu Cheng, et al. (ApJ)

massive filaments in distant high-mass star forming clouds
ALMA band 3/6+VLA K band
8 targets
(1)VLA NH_3でaspect ratio>5,
(2)L>5x$10^3L_\odot$, M>$10^3M_\odot$
(3)3.8kpc < D < 5.4kpc
ALMA band6 H2CO, SiO, CO, N2D+
VLA NH3(J,K)=(1,1),(2,2)

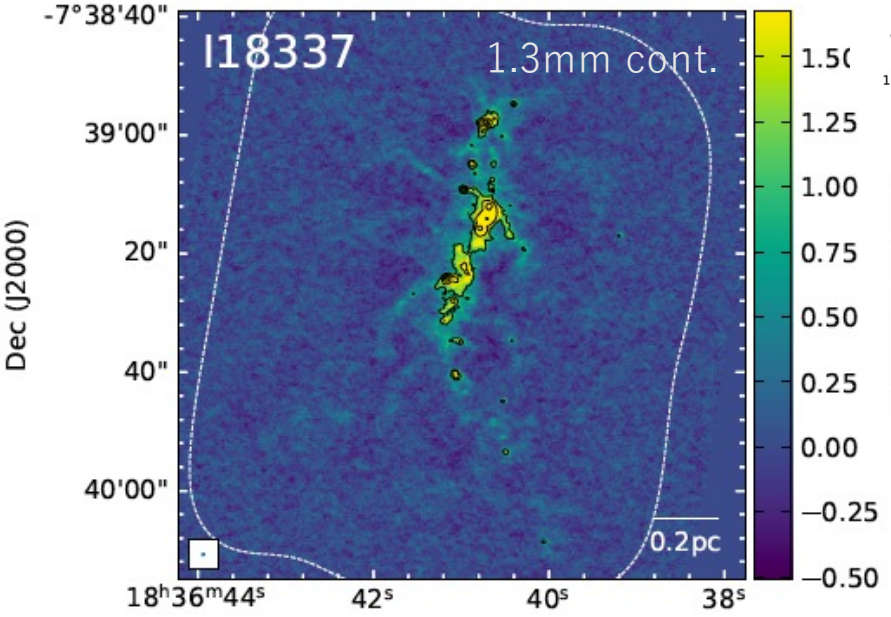

core id by *getsf* method

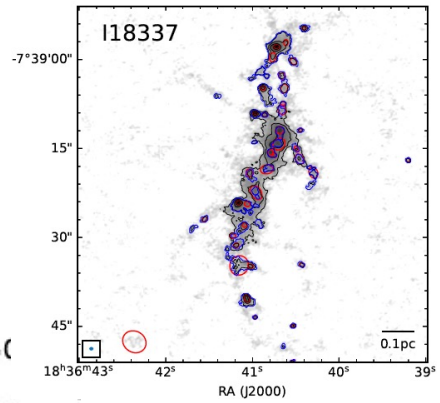

8 targetsで183 cores

Tgas from NH3 (1,1) (2,2)line ratio

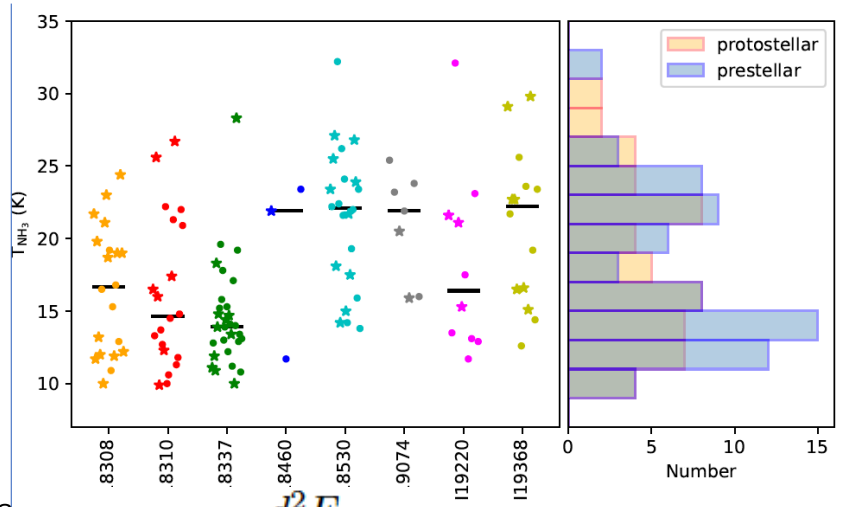

$$M_{\rm dust} = \frac{d^2 F_\nu}{\kappa_\nu B_\nu(T_{\rm dust})}.$$

(1) CO2-1,SiO5-4,SO,H2CO,CH3OHで分子流探査
43/183 with outflow
(2) H2CO warm core tracers
70cores/38coresは(1)と重複
} protostar 75/prestellar 108/183

the young group includes I18308, I18337 and I18460(∵L/M=9.3,4.9,7.6); and the evolved group includes I185
I19074 and I19220(∵L/M=11.2,11.4,12.7; compact 1.3mm emission).

core-fedかclump-fedか？

--high mass, gravitationally bound, pre-stellar cores as predicted by the core accretion theories

---- none of them has been confirmed as bona-fide high-mass prestellar cores

本研究で最大星なしコアはc2 in I 18337 M~10.3$M_{\odot}$

there are no high-mass prestellar cores in this survey.

-- substantial growth in core mass after their initial formation?

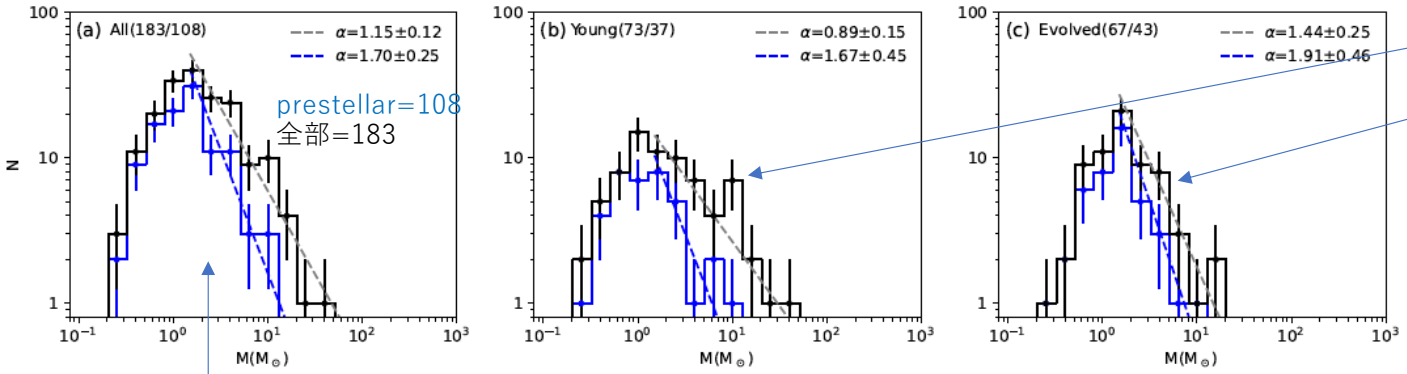

若いフィラメント
α=0.89±0.15
進化したフィラメント
α=1.44±0.25
high massに選択的に膠着するのと無矛盾？

dynamic cluster formation scenarioで説明可

we can not say with certainty whether the turnover seen in the CMF is physically real or due to incompleteness

全体α=1.15±0.12
星なしα=1.70±0.25
if high-mass cores accrete more efficiently than low-mass cores

19. Mid-Infrared Spectrum of the Disk around the Forming Companion GQ Lup B Revealed by JWST/MIRI by Gabriele Cugno, et al.

GQ Lup B is a forming brown dwarf companion ($M \sim 10-30\ M_{\rm J}$) showing evidence for an infrared excess associated with a disk surronding the companion itself. Here we present mid-infrared (MIR) observations of GQ Lup B with the Medium Resolution Spectrograph (MRS) on JWST, spanning 4.8–11.7 μm. We remove the stellar contamination using reference differential imaging based on principal component analysis (PCA), demonstrating that the MRS can perform high-contrast science. Our observations provide a sensitive probe of the disk surrounding GQ Lup B. We find no sign of a silicate feature, similar to other disk surrounding very low mass objects, which likely implies significant grain growth ($a_{\rm min} \gtrsim 5\ \mu$m), and potentially dust settling. Additionally, we find that if the emission is dominated by an inner wall, the disk around the companion might have an inner cavity larger than the one set by sublimation. Conversely, if our data probe the emission from a thin flat disk, we find the disk to be very compact. More observations are required to confirm this findings and assess the vertical structure of the disk. This approach paves the path to the future study of circumplanetary disks and their physical properties. Our results demonstrate that MIR spectroscopic observations can reveal the physical characteristics of disks around forming companions, providing unique insights into the formation of giant planets, brown dwarfs and their satellites.

20. JWST/NIRCam Imaging of Young Stellar Objects. II. Deep Constraints on Giant Planets and a Planet Candidate Outside of the Spiral Disk Around SAO 206462 by Gabriele Cugno, et al. (ApJ)

We present JWST/NIRCam F187N, F200W, F405N and F410M direct imaging data of the disk surrounding SAO 206462. Previous images show a very structured disk, with a pair of spiral arms thought to be launched by one or more external perturbers. The spiral features are visible in three of the four filters, with the non-detection in F410M due to the large detector saturation radius. We detect with a signal-to-noise ratio of 4.4 a companion candidate (CC1) that, if on a coplanar circular orbit, would orbit SAO 206462 at a separation of ~ 300 au, 2.25σ away from the predicted separation for the driver of the eastern spiral. According to the BEX models, CC1 has a mass of $M_{\rm CC1} = 0.8 \pm 0.3\ M_{\rm J}$. No other companion candidates were detected. At the location predicted by simulations of both spirals generated by a single massive companion, the NIRCam data exclude objects more massive than $\sim 2.2\ M_{\rm J}$ assuming the BEX evolutionary models. In terms of temperatures, the data are sensitive to objects with $T_{\rm eff} \sim 650-850$ K, when assuming planets emit like blackbodies ($R_{\rm p}$ between 1 and $3R_{\rm J}$). From these results, we conclude that if the spirals are driven by gas giants, these must be either cold or embedded in circumplanetary material. In addition, the NIRCam data provide tight constraints on ongoing accretion processes. In the low extinction scenario we are sensitive to mass accretion rates of the order $\dot{M} \sim 10^{-9} M_{\rm J}\ {\rm yr}^{-1}$. Thanks to the longer wavelengths used to search for emission lines, we reach unprecedented sensitivities to processes with $\dot{M} \sim 10^{-7} M_{\rm J}\ {\rm yr}^{-1}$ even towards highly extincted environments ($A_{\rm V} \approx 50$ mag).

21. Climbing the Cliffs: Classifying YSOs in the Cosmic Cliffs JWST Data using a Probabilistic Random Forest by B. L. Crompvoets, et al. (ApJ)

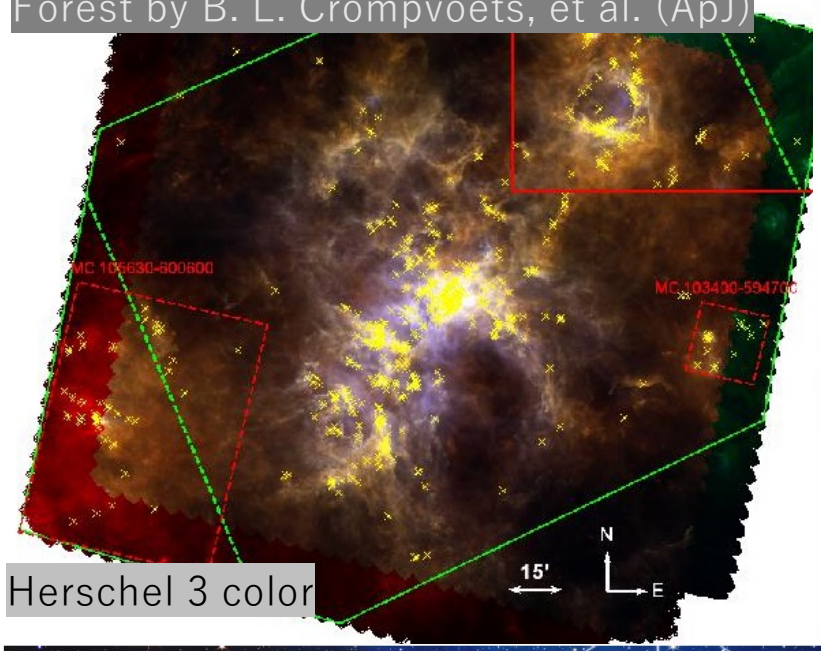

Herschel 3 color

Herschel 70μm unsharp masked

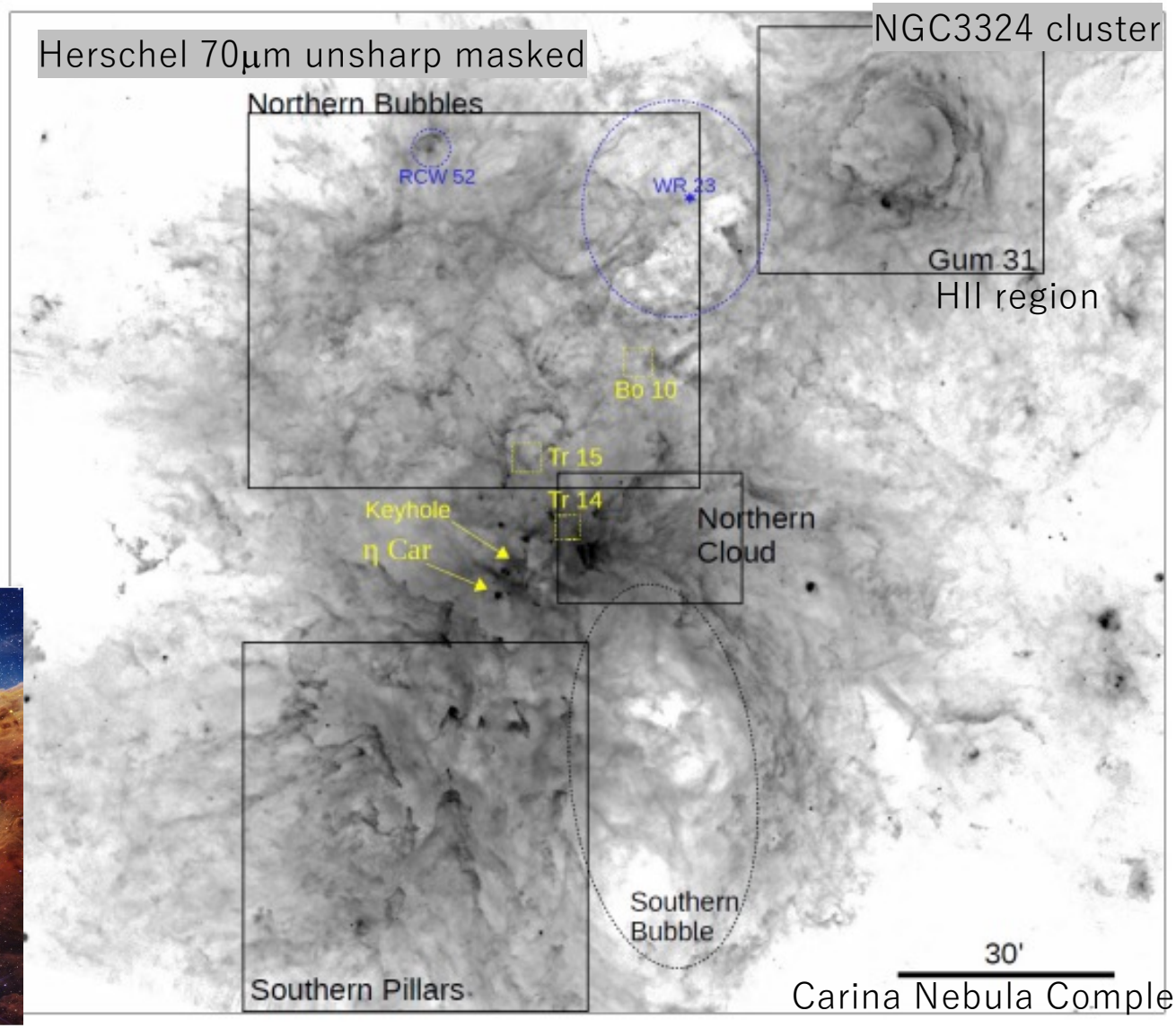

Carina Nebula Complex

22. Full orbital solutions in pre-main sequence high-order multiple systems: GG Tau Ab and UX Tau B, by Gaspard Duchêne, et al. (AAp)

Context. High-order multiple (triple and beyond) systems are relatively common. Their interaction with circumstellar and circumbinary material can have a large impact on the formation and evolution of planetary systems and depends on their orbital properties.
Aims. GG Tau and UX Tau are two pre-main sequence high-order multiple systems in which the tightest pair has a projected separation of $\approx$ 5–20 au. Characterizing precisely their orbits is crucial to establish their long-term stability, to predict the dynamics and evolution of circumstellar matter, and to evaluate the potential for planet formation in such systems.
Methods. We combine existing astrometric measurements with previously unpublished high-resolution observations of the GG Tau Ab and UX Tau B pairs and perform Keplerian orbital fits.
Results. For GG Tau Ab the data presented here represent the first detection of orbital motion. For both systems they yield dramatic increases in orbital coverage ($\gtrsim$ 60% and $\approx$ 100% for UX Tau B and GG Tau Ab, for orbital periods of $\approx$ 32 and $\approx$ 8 yr, respectively) and allow us to obtain well-constrained orbital fits, including dynamical masses with $\lesssim$ 10% and $\lesssim$ 7% random and systematic uncertainties. We find that both GG Tau A and UX Tau A–B likely form stable hierarchical systems, although one possible deprojection solution for GG Tau is strongly misaligned and could experience von Zeipel-Lidov-Kozai oscillations. We further find that the UX Tau B orbit is much more eccentric than the GG Tau Ab one, possibly explaining the lack of circumstellar material in the former.
Conclusions. The newly-determined orbits revive the question of the dynamical fate of gas and dust in these two hierarchical systems and should spur new dedicated simulations to assess the long-term evolution of the systems and the dynamical perturbations imposed by the close binaries they host.

23. Planet Formation by Gas-Assisted Accretion of Small Solids, by Gennaro D'Angelo, Peter Bodenheimer (ApJ)

We compute the accretion efficiency of small solids, with radii $1\,\mathrm{cm} \leq R_s \leq 10\,\mathrm{m}$, on planets embedded in gaseous disks. Planets have masses $3 \leq M_p \leq 20$ Earth masses ($M_\oplus$) and orbit within 10 au of a solar-mass star. Disk thermodynamics is modeled via three-dimensional radiation-hydrodynamic calculations that typically resolve the planetary envelopes. Both icy and rocky solids are considered, explicitly modeling their thermodynamic evolution. The maximum efficiencies of $1 \leq R_s \leq 100\,\mathrm{cm}$ particles are generally $\lesssim 10\%$, whereas 10 m solids tend to accrete efficiently or be segregated beyond the planet's orbit. A simplified approach is applied to compute the accretion efficiency of small cores, with masses $M_p \leq 1\,M_\oplus$ and without envelopes, for which efficiencies are approximately proportional to $M_p^{2/3}$. The mass flux of solids, estimated from unperturbed drag-induced drift velocities, provides typical accretion rates $dM_p/dt \lesssim 10^{-5}\,M_\oplus\,\mathrm{yr}^{-1}$. In representative disk models with an initial gas-to-dust mass ratio of 70–100 and total mass of 0.05–0.06 $M_\odot$, solids' accretion falls below $10^{-6}\,M_\oplus\,\mathrm{yr}^{-1}$ after 1–1.5 Myr. The derived accretion rates, as functions of time and planet mass, are applied to formation calculations that compute dust opacity self-consistently with the delivery of solids to the envelope. Assuming dust-to-solid coagulation times of ≈ 0.3 Myr and disk lifetimes of ≈ 3.5 Myr, heavy-element inventories in the range 3–7 $M_\oplus$ require that ≈ 90–$150\,M_\oplus$ of solids cross the planet's orbit. The formation calculations encompass a variety of outcomes, from planets a few times $M_\oplus$, predominantly composed of heavy elements, to giant planets. The peak luminosities during the epoch of solids' accretion range from $\approx 10^{-7}$ to $\approx 10^{-6}\,L_\odot$.

24. The jet of BP Tau, by A. V. Dodin, et al. (AApL)

Context. A strong global magnetic field of young low-mass stars and a high accretion rate are the necessary conditions for the formation of collimated outflows (jets) from these objects. But it is still unclear whether these conditions are also sufficient.
Aims. We aim to check whether BP Tau, an actively accreting young star with a strong magnetic field, has a jet.
Methods. We carried out narrowband [S II] 672 nm imaging and spectroscopic observations of BP Tau and its vicinity.
Results. We find that BP Tau is a source of a Herbig-Haro flow (assigned number HH 1181), which includes two HH objects moving from the star in opposite directions and a micro- (counter-) jet of $\sim$ 1″ projected length. The flow is oriented along position angle $59 \pm 1°$.

25. The stability of dense cores near the Serpens South protocluster, by Rachel K. Friesen, Emma Jarvis (ApJ)

Most stars form in clusters and groups rather than in isolation. We present $\lesssim 5''$ angular resolution ($\sim$ 2000 au, or 0.01 pc) Very Large Array NH_3 (1,1), (2,2), and (3,3) and 1.3 cm continuum emission observations of the dense gas within the Serpens South protocluster and extended filaments to the north and south. We identify 94 dense cores using a dendrogram analysis of the NH_3 (1,1) integrated intensity. Gas temperatures T_K and non-thermal linewidths σ_{NT} both increase towards the centre of the young stellar cluster, in the dense gas generally and in the cores specifically. We find that most cores (54%) are super-virial, with gravitationally bound cores located primarily in the filaments. Cores in the protocluster have higher virial parameters by a factor ~ 1.7, driven primarily by the increased core σ_{NT} values. These cores cannot collapse to form stars unless they accrete additional mass or their core internal motions are reduced. The southern filament shows a significant velocity gradient previously interpreted as mass flow toward the cluster. We find more complex kinematics in the northern filament. We find a strong correlation between σ_{NT} and T_K, and argue that the enhanced temperatures and non-thermal motions are due to mechanical heating and interaction between the protocluster-driven outflows and the dense gas. Filament-led accretion may also contribute to the increased σ_{NT} values. Assuming a constant fraction of core mass ends up in the young stars, future star formation in the Serpens South protocluster will shift to higher masses by a factor ~ 2.

26. MINDS: Mid-infrared atomic and molecular hydrogen lines in the inner disk around a low-mass star by Riccardo Franceschi, at al. (AAp)

Context. Understanding the physical conditions of circumstellar material around young stars is crucial to star and planet formation studies. In particular, very low-mass stars ($M_\star < 0.2$ $M_\odot$) are interesting sources to characterize as they are known to host a diverse population of rocky planets. Molecular and atomic hydrogen lines can probe the properties of the circumstellar gas.

Aims. This work aims to measure the mass accretion rate, the accretion luminosity, and more generally the physical conditions of the warm emitting gas in the inner disk of the very low-mass star 2MASS-J16053215-1933159. We investigate the source mid-infrared spectrum for atomic and molecular hydrogen line emission.

Methods. We present the full James Webb Space Telescope (JWST) Mid-InfraRed Instrument (MIRI) Medium Resolution Spectrometer (MRS) spectrum of the protoplanetary disk around the very low-mass star 2MASS-J16053215-1933159 from the MINDS GTO program, previously shown to be abundant in hydrocarbon molecules. We analyzed the atomic and molecular hydrogen lines in this source by fitting one or multiple Gaussian profiles. We then built a rotational diagram for the H_2 lines to constrain the rotational temperature and column density of the gas. Finally, we compared the observed atomic line fluxes to predictions from two standard emission models.

Results. We identify five molecular hydrogen pure rotational lines and 16 atomic hydrogen recombination lines in the 5 to 20 μm spectral range. The spectrum indicates optically thin emission for both species. We use the molecular hydrogen lines to constrain the mass and temperature of the warm emitting gas. We derive a total gas mass of only 2.3×10^{-5} M_{Jup} and a temperature of 635 K for the warm H_2 gas component located in the very inner disk ($r < 0.033$ au), which only accounts for a small fraction of the upper limit for the disk mass from continuum observations (0.2 M_{Jup}). The HI (7-6) recombination line is used to measure the mass accretion rate (4.0×10^{-10} $M_\odot$ yr^{-1}) and luminosity (3.1×10^{-3} $L_\odot$) onto the central source. This line falls close to the HI (11-8) line, however at the spectral resolution of JWST MIRI we managed to measure both separately. Previous studies based on Spitzer have measured the combined flux of both lines to measure accretion rates. HI recombination lines can also be used to derive the physical properties of the gas using atomic recombination models. The model predictions of the atomic line relative intensities constrain the atomic hydrogen density to about $10^9 - 10^{10}$ cm^{-3} and temperatures up to 5 000 K.

Conclusions. The JWST-MIRI MRS observations for the very low-mass star 2MASS-J16053215-1933159 reveal a large number of emission lines, many originating from atomic and molecular hydrogen because we are able to look into the disk warm molecular layer. Their analysis constrains the physical properties of the emitting gas and showcases the potential of JWST to deepen our understanding of the physical and chemical structure of protoplanetary disks.

27. An ALMA search for substructure and fragmentation in starless cores in Orion B North, by Samuel Fielder, et al. (ApJ)

We present Atacama Large Millimeter/submillimeter Array (ALMA) Cycle 3 observations of 73 starless and protostellar cores in the Orion B North molecular cloud. We detect a total of 34 continuum sources at 106 GHz, and after comparisons with other data, 4 of these sources appear to be starless. Three of the four sources are located near groupings of protostellar sources, while one source is an isolated detection. We use synthetic observations of a simulation modeling a collapsing turbulent, magnetized core to compute the expected number of starless cores that should be detectable with our ALMA observations and find at least two (1.52) starless core should be detectable, consistent with our data. We run a simple virial analysis of the cores to put the Orion B North observations into context with similar previous ALMA surveys of cores in Chamaeleon I and Ophiuchus. We conclude that the Chamaeleon I starless core population is characteristically less bounded than the other two populations, along with external pressure contributions dominating the binding energy of the cores. These differences may explain why the Chamaeleon I cores do not follow turbulent model predictions, while the Ophiuchus and Orion B North cores are consistent with the model.

28. A self-consistent model for dust settling and the vertical shear instability in protoplanetary disks, by Yuya Fukuhara, Satoshi Okuzumi (PASJ)

The spatial distribution of dust particles in protoplanetary disks affects dust evolution and planetesimal formation processes. The vertical shear instability (VSI) is one of the candidate hydrodynamic mechanisms that can generate turbulence in the outer disk region and affect dust diffusion. Turbulence driven by the VSI has a predominant vertical motion that can prevent dust settling. On the other hand, the dust distribution controls the spatial distribution of the gas cooling rate, thereby affecting the strength of VSI-driven turbulence. Here, we present a semi-analytic model that determines the vertical dust distribution and the strength of VSI-driven turbulence in a self-consistent manner. The model uses an empirical formula for the vertical diffusion coefficient in VSI-driven turbulence obtained from our recent hydrodynamical simulations. The formula returns the vertical diffusion coefficient as a function of the vertical profile of the cooling rate, which is determined by the vertical dust distribution. We use this model to search for an equilibrium vertical dust profile where settling balances with turbulent diffusion for a given maximum grain size. We find that if the grains are sufficiently small, there exists a stable equilibrium dust distribution where VSI-driven turbulence is sustained at a level of $\alpha_z \sim 10^{-3}$, where α_z is the dimensionless vertical diffusion coefficient. However, as the maximum grain size increases, the equilibrium solution vanishes because the VSI can no longer stop the settling of the grains. This runaway settling may explain highly settled dust rings found in the outer part of some protoplanetary disks.

29. Gaia23bab : a new Exor, by T. Giannini, et al. (ApJ)

On March 6 2023, the Gaia telescope has alerted a 2-magnitude burst from Gaia23bab, a Young Stellar Object in the Galactic plane. We observed Gaia23bab with the Large Binocular Telescope obtaining optical and near-infrared spectra close in time to the peak of the burst, and collected all public multi-band photometry to reconstruct the historical light curve. This latter shows three bursts in ten years (2013, 2017 and 2023), whose duration and amplitude are typical of EXor variables. We estimate that, due to the bursts, the mass accumulated on the star is about twice greater than if the source had remained quiescent for the same period of time. Photometric analysis indicates that Gaia23bab is a Class II source with age $\lesssim 1$ Myr, spectral type G3−K0, stellar luminosity ~ 4.0 $L_\odot$, and mass ~ 1.6 $M_\odot$. The optical/near infrared spectrum is rich in emission lines. From the analysis of these lines we measured the accretion luminosity and the mass accretion rate ($L_{\rm acc}{}^{burst} \sim 3.7$ $L_\odot$, $\dot{M}_{\rm acc}{}^{burst} \sim 2.0 \times 10^{-7}$ $M_\odot\,{\rm yr}^{-1}$) consistent with those of EXors. More generally, we derive the relationships between accretion and stellar parameters in a sample of EXors. We find that, when in burst, the accretion parameters become almost independent of the stellar parameters and that EXors, even in quiescence, are more efficient than classical T Tauri stars in assembling mass.

30. Reduction of dust radial drift by turbulence in protoplanetary disks, by Fabiola Antonietta Gerosa, et al. (AAp)

Context. Dust particles in protoplanetary disks rotate at velocities exceeding those of the surrounding gas due to a lack of pressure support. Consequently, they experience a head-wind from the gas that drives them toward the central star. Radial drift occurs on timescales much shorter than those inferred from disk observations or those required for dust to aggregate and form planets. Additionally, turbulence is often assumed to amplify the radial drift of dust in planet-forming disks when modeled through an effective viscous transport. However, the local interactions between turbulent eddies and particles are known to be significantly more intricate than in a viscous fluid.

Aims. Our objective is to elucidate and characterize the dynamic effects of Keplerian turbulence on the mean radial and azimuthal velocities of dust particles.

Methods. We employ 2D shearing-box incompressible simulations of the gas, which is maintained in a developed turbulent state while rotating at a sub-Keplerian speed. Dust is modeled as Lagrangian particles set at a Keplerian velocity, therefore experiencing a radial force toward the star through drag.

Results. Turbulent eddies are found to reduce the radial drift, while simultaneously enhancing the azimuthal velocities of small particles. This dynamic behavior arises from the modification of dust trajectories due to turbulent eddies.